Microporous and Mesoporous Materials 228 (2016) 207–214

Contents lists available at ScienceDirect

Microporous and Mesoporous Materials

journal homepage: www.elsevier.com/locate/micromeso

Antiphlogistic effect by zeolite as determined by a murine inflammation model

Javiera Cervini-Silva [a, b, c, *], Antonio Nieto-Camacho [d], Stephan Kaufhold [e], Kristian Ufer [e], Eduardo Palacios [f], Ascención Montoya [g], Wilfried Dathe [h, **]

[a] Departamento de Procesos y Tecnología, Universidad Autónoma Metropolitana Unidad Cuajimalpa, México City, Mexico
[b] Earth Sciences Division, Lawrence Berkeley National Laboratory, Berkeley, CA, USA
[c] NASA Astrobiology Institute, USA
[d] Laboratorio de Pruebas Biológicas, Instituto de Química, Universidad Nacional Autónoma de México, Ciudad Universitaria México City, Mexico
[e] BGR Bundesanstalt für Geowissenschaften und Rohstoffe, Stilleweg 2, D-30655, Hannover, Germany
[f] Departamento de Microscopía Electrónica, Instituto Mexicano del Petróleo, Mexico City, Mexico
[g] Dirección de Investigación y Posgrado, Instituto Mexicano del Petróleo, Mexico City, Mexico
[h] Heck Bio-Pharma GmbH, Gerberstraße 15, D-73650, Winterbach, Germany

ARTICLE INFO

Article history:
Received 20 February 2016
Received in revised form
24 March 2016
Accepted 29 March 2016
Available online 1 April 2016

Keywords:
Clinoptilolite
Histamine
Adsorption

ABSTRACT

Natural zeolites are microporous crystalline aluminosilicates with channels and cavities of molecular dimensions of interest for biomedical applications. The antiphlogistic effect was investigated on the basis of a murine inflammation model using 12-*O*-tetradecanoylphorbol-13-acetate (TPA) as inflammatory agent and the quantification of the activity of myeloperoxidase (MPO), an enzyme that serves as an indicator for neutrophil migration.

The zeolite used in this study was collected from San Andrés, Cuba, and it provided evidence to show the quantitative adsorption of histamine, a biogenic compound strongly involved in inflammation processes. Furthermore, a related work showed that this zeolite sample is free of hazardous materials and apt for health use. The zeolite of this study contained 65% clinoptilolite, 30% mordenite, and 5% smectite. The application of this zeolite reduced the edema formation induced by TPA within 24 h by 57.2 ± 18%, while the migration of neutrophils was not altered. The anti-inflammatory activity of zeolite was explained in part due to the quantitative adsorption of histamine, whilst natural cell repair mechanisms appeared not to be influenced. The outcome of this work expanded on reports concluding that antiphlogistic properties of zeolite proven *in vivo* with mice for inflammatory diseases are important for both oral application (gastrointestinal tract) and topical treatment (skin), too.

1. Introduction

1.1. Structure and biological activity of zeolite minerals

Natural zeolites are microporous crystalline aluminosilicates with channels and cavities of molecular dimensions, allowing for adsorption, ion exchange, water sorption/desorption, molecular sieving and excellent binding capacity for toxins and other harmful substances.

Of particular interest herein is the use of zeolites in biomedical applications, namely as active ingredients in medical devices, carriers for drugs like antibiotics, wound healing accelerators, adjuvants in anticancer therapy and several other applications [1,2]. To avoid deleterious effect(s) on health and recommending their use, however, scrutiny on mineralogical, chemical and microbiological characterization becomes necessary and should be the base for oral application on the updated rules of the International Pharmacopoeias [3]. In particular, it is of interest to provide information whether naturally occurring hazardous minerals such as fibrous zeolite erionite may be present (IARC, 2012). Amongst the more than 40 zeolites occurring naturally, clinoptilolite, $[(Na,K)_{6-2x}Ca_x]$

* Corresponding author. Departamento de Procesos y Tecnología, Universidad Autónoma Metropolitana, Unidad Cuajimalpa, Av. Vasco de Quiroga 4871, Del. Cuajimalpa, Col. Santa Fe, C.P. 05348, México, D.F., Mexico.
** Corresponding author.
E-mail addresses: jcervini@correo.cua.uam.mx (J. Cervini-Silva), daweidoc@gmx.de (W. Dathe).

http://dx.doi.org/10.1016/j.micromeso.2016.03.043
1387-1811/

$(A1_6Si_{30}O_{72})\cdot 24H_2O$, is the most abundant in soils and sediments (Ming and Mumpton, 1987), and has been used traditionally in the preparation of a large number of nutritional and/or dietary supplements and biomedical applications [2,4–6].

Clinoptilolite is a natural zeolite of the heulandite group with a two-dimensional channel system formed by 10-ring (0.31 nm × 0.75 nm [001]) and 8-ring (0.36 nm × 0.46 nm [001] and 0.28 nm × 0.47 nm [100]) channels [7] that act as a selective cation exchanger. For instance, clinoptilolite exchanged Na^+ for NH_4^+ but not for $(CH_3)_3CNH_3^+$, a signature that few of the charged sites are accessible to large organic ions [8]. Furthermore, most of the surface charge arises from external surface sites (i.e., non-channel sites) and half-cage sites, both of which are exchange sites in proximity to the aperture of a channel where larger organic ions (e.g., $(CH_3)_3CNH_3^+$) have access *albeit* partial. Last but not least, particle size may alter contribution to surface charge by half-cage and external surface sites [8]. Taken together, the aforementioned properties are subject of interest in the present study. In particular, a related study reported that zeolite from San Andrés, Cuba (22°40′14″N 83°34′05″O), composed primarily by clinoptilolite and mordenite, showed a high binding capacity of histamine, a neurotransmitter critical to the inflammatory response and pruritus [9]. The adsorption of histamine at pH 1 and 7 was 12 and 16 mg per g of zeolite, respectively. It is worth mentioning that the zeolite sample studied herein was composed primarily by medium-pore sized clinoptilolite (see above) and large-pore sized mordenite, 12-ring channels, pore size 0.65 × 0.70 nm [10].

1.2. Principles of edema

Edema forms due to increases of liquid level within the stroma, changes of vascular permeability, especially capillaries, and it is frequently associated to increased histamine levels as well as to the up-regulation of pro-inflammatory substances (e.g., cytokines IL-1, IL-6, and TNF-α; [11]). Most recently, a simultaneous decrease of the pro-inflammatory substances and the reduction of ear edema confirmed the antiphlogistic factor of a citrus flavonoid [12].

This manuscript presents evidence of the anti-inflammatory activity of zeolite from San Andrés, Cuba, in a murine inflammation model. Reportedly, this zeolite sample can adsorb up to 16 mg of histamine per g under physiological conditions [10]. The aforementioned results served as basis to postulate that the antiphlogistic activity of the zeolite was attributed at least in part to the preferred retention of histamine over other pro-inflammatory compounds such as interleukins (IL). Interleukins are hormones, small proteins, of the immunological system and belong to the cytokines. Pertinent examples include the pro-inflammatory cytokines IL-1 and IL-6, consisting of 153 and 185 amino acids, respectively [13,14]. Consequently, these cytokines surpass in dimension channels and cavities typically found in clinoptilolite or mordenite mineral structure, guaranteeing cytokine exclusion from internal microporous sites.

The anti-inflammatory activity of clays and clay minerals has been tested in a murine inflammation model, whereby indomethacin, a commercial non-steroidal anti-inflammatory drug (NSAID), was selected as reference. Indomethacin prevented TPA induced edema by means of reducing the concentration of pro-inflammatory compounds, including cytokines [15]. In those studies, the effect of clays and clay minerals on the migration of neutrophils [polymorphonuclear (PMN) leukocytes] which, after the skin, constitute the primary protection of organisms against pathogens. In the present manuscript the authors compared the anti-inflammatory activity of zeolite and that reported for clays and clay minerals (e.g., [16–22]).

1.3. Inflammation and migration of neutrophils

Acute inflammation is the first reaction of an organism to defend against outside attack(s) by microorganisms or toxic compounds and belongs to an effective natural repair mechanism. Foreign substances induce a regulatory cascade triggering chemotaxis of leukocytes, primarily as neutrophils, which are first at reaching the site of invading antigen [23]. Neutrophils release myeloperoxidase (MPO) by a degranulation process, reacting with H_2O_2 formed by the respiratory burst to form a complex that can oxidize a large variety of substances and provoking a rapid microbicidal effect [24]. Therefore, the quantification of MPO is considered a good marker for neutrophil infiltration into an inflamed tissue [25]. This paper reports on the anti-inflammatory activity of zeolite.

1.4. Antiphlogistic and antibacterial characteristics

Because microorganisms cause many inflammation processes, the antiphlogistic and antibacterial characteristics are in many cases entangled. On the one hand, studies reported the antibacterial activity of clays based on their effect on growth and membrane stability of bacteria, concluding that bactericidal clays contain soluble reduced metals and expandable clay minerals that absorb cations, providing a capacity for extended metal release and production of toxic hydroxyl radicals, whereby soluble Fe^{3+}, Fe^{2+}, and Al^{3+} were reported to be the critical antibacterial components [26,27]. On the other hand, reports on the antiphlogistic activity focused on the clinical effects of minerals on inflamed tissue [16–22]. A wide array of clays and clay minerals (e.g., allophane, halloysite, bentonites, sepiolite, palygorskite), expandable or non-expandable, containing labile Al or Fe, or not, inhibited edema and myeloperoxidase content. Whilst labile metals ions contribute to the anti-inflammatory activity of clays and clay minerals, evidence collected until to date support the idea that structural commonalities amongst them become limiting for transport and, ultimately, for an effective edema inhibition and infiltration of different leukocyte cells to an inflammation site [16–22,28], subsequently allowing for resolution of inflammation, whereby macrophages participated in anti-inflammatory mechanisms leading to the return to homeostasis in tissues [28].

2. Materials and methods

2.1. Materials

Zeolite was collected from San Andrés, Cuba (22°40′14″N 83°34′05″O) and used as received without further treatment. The average particle size was about 40 μm [10].

Hydrochloric acid (HCl, 32%), buffer solution (Dulbecco's Phosphate Buffered Saline, DPBS, without Ca and Mg) and histamine (97%) were purchased from Merck, Lonza and Sigma-Aldrich, respectively.

2.2. Sample characterization

2.2.1. X-ray diffraction (XRD)

XRD patterns were recorded using a PANalytical X'Pert PRO MPD Θ-Θ diffractometer (Cu-Kα radiation generated at 40 kV and 40 mA), equipped with a variable divergence slit (20 mm irradiated length), primary and secondary soller, diffracted beam monochromator, and a point detector. The samples in air-dried condition were investigated from 1° to 55° 2Θ with a step size of 0.03° 2Θ and a measuring time of 6 s per step.

Furthermore, the specimens were stored overnight in an ethylene glycol atmosphere at 60 °C. The sample films were

measured from 1° to 55° 2Θ (stepsize 0.03° 2Θ, 6 s per step) after cooling to room temperature, representing EG conditions.

The quantitative mineralogical composition was calculated based on XRD pattern recorded by a PANalytical X'Pert PRO MPD Θ-Θ diffractometer (Co-Kα radiation generated at 40 kV and 40 mA), equipped with a variable divergence slit (20 mm irradiated length), primary and secondary soller, diffracted beam monochromator, and a point detector. After back loading preparation the samples were investigated from 2° to 90° 2Θ with a step size of 0.03° 2Θ and a measuring time of 3 s per step in air-dried condition. Pattern were refined using the Rietveld-code BGMN.

To identify trace amounts of clay minerals oriented mounts were prepared again, and analysed by XRD. Fifteen mg per cm^2 sample was used to record an XRD scan. An aliquot of 1.5 mL of sample suspension was deposited on the circular (diameter = 2.4 cm) ceramic tiles which were 3-mm thick. The suspension was filtered through the tile using a vacuum filter apparatus.

2.2.2. X-ray fluorescence

X-ray fluorescence analysis of powdered samples was conducted using a PANalytical Axios spectrometer (ALMELO, The Netherlands). Samples were prepared by mixing with a flux material (lithium metaborate Spectroflux, Flux No. 100A, Alfa Aesar) and melting into glass beads. The beads were analyzed by wavelength-dispersive XRF. To determine loss on ignition (LOI), 1000 mg of sample material were heated to 1030 °C for 10 min.

2.2.3. Specific surface area

Specific surface area determinations were conducted by N_2 adsorption using a 5 point BET method, by placing 30 mg of sample inside a Micrometrics Gemini III 2375 surface area analyzer. Prior to specific surface area determinations, to remove adsorbed water the zeolite sample was degassed under vacuum at 105 °C for 24 h.

2.2.4. Cation exchange capacity

The CEC was measured using the Cu-triethylenetetramine method [29].

2.2.5. Thermogravimetric analyses

Thermoanalytical investigations were performed using a Netzsch 449 F3 Jupiter thermobalance equipped with a DSC/TG sample holder linked to a Netzsch QMS 403 C Aeolus mass spectrometer (MS). One hundred mg of powdered material previously equilibrated at 53% relative humidity (RH) was heated from 25 to 1150 °C at a heating rate of 10 K/min.

2.2.6. Water absorption capacity

The water adsorption capacity was measured using the Dieng-modified Enslin-Neff device [30]. In addition, the water adsorption was determined after equilibration of 500 mg powder at 50 and 70% R.H, respectively. The relative humidity was controlled by a climate oven. A detailed description of the methodology can be found elsewhere [31].

2.2.7. High resolution electron microscopy

High-resolution transmission electron microscopy (HRTEM) analyses were conducted using a TITAN 80–300 (FEI) set at 300 kV and 0.01 nm resolution, and equipped with a Cs corrector from CEOS. The chemical composition of specimens was determined using a JEOL 2010 TEM (200 kV, a 0.195 nm point-to-point resolution, and a 90.0° take-off angle) equipped with a Link-Isis energy dispersive spectroscopy (EDS) detector. All experiments were conducted in quintuplicate. Scanning electron microscopy and energy dispersive spectroscopy (SEM-EDS) analyses were conducted by placing samples in an aluminum sample holder and fixed with carbon tape. SEM analyses were conducted using a Nova-200 Nanolab double-beam SWM, with ~1.1 nm resolution, coupled with an EDS for microanalyses.

2.3. Biological tests

2.3.1. Animals

Adult male CD-1 mice (25–30 g) approved by the Animal Care and Use Committee (NOM-062-ZOO-1999) were provided by the Instituto de Fisiología Celular, UNAM. They were maintained at 25 °C on a 12/12 h light-dark cycle with free access to food and water.

2.3.2. Mouse-ear edema method

Determinations of the mouse ear edema using 12-*O*-tetradecanoylphorbol-13-acetate (TPA) as the inflammatory agent were conducted according to methods described elsewhere [32]. Briefly, a group of five to ten male CD1 mice were anesthetized using Sedaphorte (32 mg kg^{-1} of sodium pentobarbital, intraperitoneal). Under complete anesthesia, 10 μL of a 0.25 mg mL^{-1} ethanolic solution of TPA was topically applied on both faces of the mouse right ear; thus, 5-μL aliquots were applied to each face. To ensure full TPA absorption, the mouse ears were let in contact with the TPA solution for 15 min before proceeding to the next experimental step. Parallel reference experiments were conducted in the left ear where only ethanol was applied.

Dispersions were prepared by adding 1 mg sample to 20 μL of 1:1 water: acetone. Aliquots of 10 μL of the freshly-prepared clay dispersion were applied to both faces of the right ear.

A parallel set of experiments to study the effect of indomethacin was conducted using a second group of animals. A solution containing 1 mg of indomethacin dissolved in 1:1 ethanol: acetone was prepared. Twenty microliter aliquots of indomethacin solution were spread on the right ear faces such that *ca.* 10 μL was applied to each face. In this case, a group of animals that served as control were exposed to the vehicle solutions, namely, either 1:1 water: acetone or 1:1 ethanol: acetone.

After 4 or 24 h of the application of dispersions containing zeolite sample, indomethacin, or vehicle, the animals remained anesthetized during either period of time, and were later sacrificed in a CO_2 chamber. All experimental procedures involving animals were handled in strict accordance with good animal practices as described above. Then, 7-mm diameter plugs were removed from each ear.

The edematous response was determined from measured plus mass difference. The edema inhibition (EI) was calculated according to:

$$EI \equiv \frac{A - B}{A} \times 100 \quad (1)$$

where A and B correspond to mass determined for samples exposed to TPA only and TPA plus indomethacin or zeolite.

EI values were determined at $t = 4$ and 24 h. Values from $p \leq 0.05$ (*) and $p \leq 0.01$ (**) were considered to differ significantly from control experiments. All results were analyzed using the t student test. In all experiments, the dose corresponded to 1 mg ear^{-1}. Results were expressed as average value with standard error. In all experiments, EI was estimated according to Eq. (1).

2.3.3. Myeloperoxidase (MPO) method

Estimations of myeloperoxidase (MPO) enzymatic activity are used in inflammation models as an enzymatic marker specific for migration and cellular infiltration [33]. This is particularly the case

Table 1
Mineralogical composition of zeolite from San Andrés, Cuba, as determined by XRD Rietveld (this study) and XRD [10].

Mineral phase	*XRD Rietveld*	*XRD*
	wt (%)	
Clinoptilolite	65	45
Mordenite	30	40
Smectite	5	Not detected
Quartz	Not detected	Traces
Anorthite	Not detected	Traces

for PMN bearing high contents of MPO. In all cases, the enzymatic activity of MPO was determined from right-ear biopsies either 4 or 24 h after exposure to TPA-containing samples as described above.

Hexadecyltrimethylammonium bromide (HTAB) was dissolved in 80 mM of a phosphate-buffered saline (PBS) solution to give a concentration of 0.5% HTAB. The pH was adjusted to 5.4. Right-ear biopsies were placed in contact with 1 mL of the freshly-prepared HTAB solution. The samples were then homogenized for 30 s at 4 °C using a Tissue Tearor Homogenizer International (OMNI model 125). The homogenized dispersions were freeze-thawed three times, sonicated for 20 s, and centrifuged at 13,400 g for 15 min at 4 °C. Ten microliter aliquots of the resulting supernatant solutions were separated and poured into microtiter plates. Subsequently, one hundred microliter aliquots of the PBS solution were added to each well.

Twenty-μL aliquots of a 0.017% hydrogen peroxide solution were added to each well, before the microtiter plates were heated at 37 °C.

A 18.4-mM 3,3′,5,5′, tetramethylbenzidine (TMB) solution in 1:1 dimetilformamide (DMF): water was prepared. Twenty microliters of the TMB solution was added to each well. The microplates were incubated at 37 °C for 5 min at a constant shaking speed of 100 r.p.m. A 20-μL aliquot of a 2 M H_2SO_4 solution was added to each well to stop the reaction.

The enzyme activity of MPO was quantified colorimetrically using a BioTek Microplate Reader (EL X 808) at $\lambda = 450$ nm. The activity of MPO was expressed as optical density per biopsy (OD/Biopsy). All experiments were conducted in quadruplicates.

3. Results and discussion

3.1. Mineralogy, texture, and morphology

XRD Rietveld determinations for zeolite showed the presence of clinoptilolite, mordenite, and smectite by 65, 30, and 5%, respectively (Table 1, Fig. 1, and Supplementary material Fig. 1A). No signature of clay minerals became evident. These findings expanded on XRD analysis reported elsewhere [10] concluding that the composition was 45% clinoptilolite and 40% mordenite. Therefore, the composition of the zeolite sample subject of study varied slightly as it can be expected in natural products. In all, the properties of the zeolite sample resembled those proper of clinoptilolite, with features typical for mordenite and smectite.

Shown in Fig. 2 are high-resolution micrographs for the zeolite sample, denoting heterogeneity in size and composition; however, no presence of fibrous mineral structures became evident, in agreement with previous work [10]. Transmission electron micrographs confirmed the presence of laminated materials (Fig. 3), a signature of clays. Based on *d*-values, these results were assigned to smectite (non-expanding 9.98 Å/partially expanding 13.5 Å layers; [34]). According to the Pharmacopoeia [3], the aforementioned characteristics for the zeolite sample from San Andrés, Cuba, met the requirements established for a hazardous-free material for human applications.

3.2. Specific surface area and cation exchange capacity

Surface area determinations conducted by N_2 adsorption using a 5 point BET method, under vacuum at 105 °C for 24 h, were relatively low (22 $m^2\ g^{-1}$) in comparison to previous determinations using an automated nitrogen adsorption analyzer at Micromeritics Analytical Services (Europe, Aachen, Germany), *ca.* 140 $m^2\ g^{-1}$ [10]. Arguably, removing water at 105 °C and 24 h prior to surface area determinations allowed for the entrance of N_2 molecules only into the largest channels but not into the small ones. Evidently, increasing pretreatment temperature (250–300 °C for several hours) allowed for higher S_{BET} values, provided the entrance of N_2 molecules into both larger and smaller channels. This was also found to be true for CEC determinations. The experimental CEC

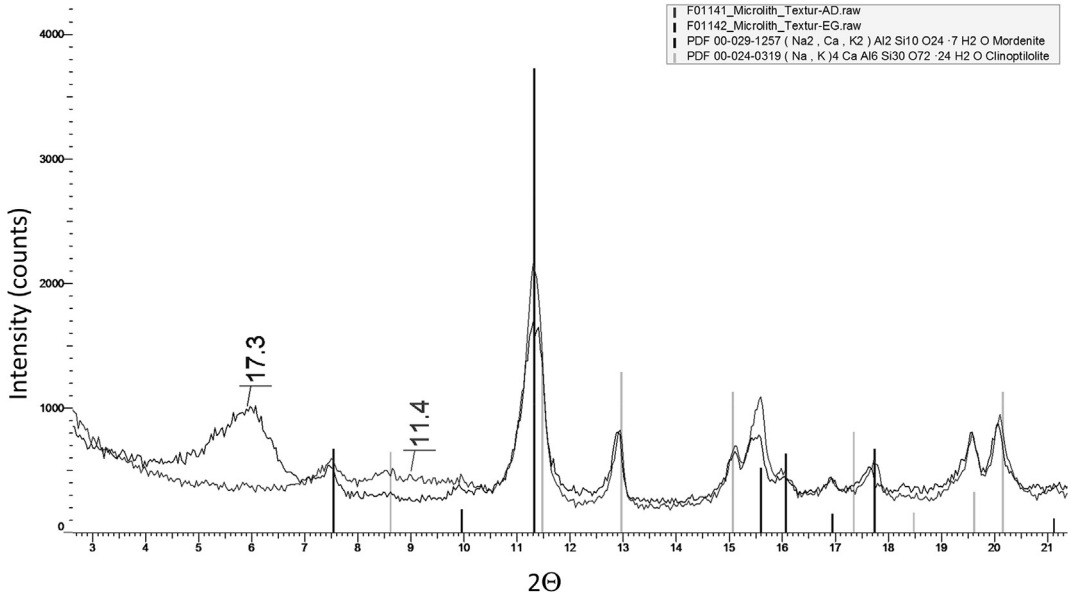

Fig. 1. XRD of zeolite from San Andrés, Cuba: oriented mount before and after and EG treated showed the presence of smectite.

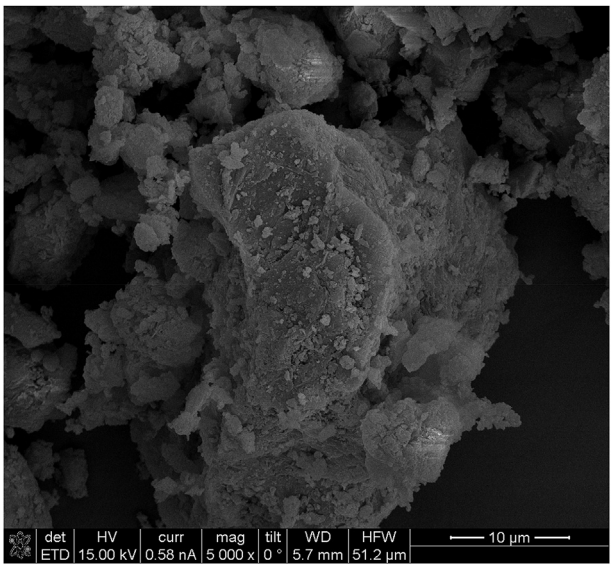

Fig. 2. HRSEM of zeolite from San Andrés, Cuba.

value for the zeolite sample (11 meq 100 g^{-1}) was found well below those reported for zeolite minerals (100 ≤ CEC ≤ 300 meq 100 g^{-1}), regardless of index cation yet strongly dependent on isomorphic substitution stemming from the amount of $A1^{3+}$ replacing Si^{4+} in the structure. Reported CEC values for clinoptilolite, and that corrected for external surface and half-cage sites approximate 175 and 165 meq 100 g^{-1} (i.e., 175–10 meq 100 g^{-1}), respectively [8]. At first glance these findings are *in lieu* with pore blocking with inorganic material, although this proposal it is difficult to assess as little information has become available on CEC values for zeolites determined by the Cu-Trien method [29].

3.3. Chemical composition and water uptake

The chemical composition of the zeolite sample was confirmed with XRF (Table 2). Results showed enrichment with Ba and Sr and, to a lesser extent, other non-toxic chemical components. The identification of traces of C- or S-phases was conducted by simultaneous gas analysis (Figs. 4 and 5). The dehydration of zeolite was noted from 100 to about 400 °C, reaching a maximum value just below 200 °C. At about 507 °C, a small peak was observed both in the DSSC and MS-H_2O curve that could be from a trace of accessory clay minerals, which arguably corresponded to smectite. In the MS-CO_2 curve, a small peak showing slightly above 600 °C pointed towards the presence of traces of carbonates, however it was considered to be free of organic impurities.

The water content after equilibration of the powder at 53% R.H. prior to thermal analysis was about 15 mass % at 600 °C (Fig. 4). The water uptake capacity was determined at 105 °C after equilibration at 50 and 70% R.H., respectively, as described elsewhere [30,31].

Water uptake increased steadily within the first 5 min, reaching a 70% value and remaining stable thereafter (Fig. 5). These results were explained by the removal of water adsorption, thus eliminating media for microbial survival [35]. Pertinent herein is a related report on the physicochemical behaviour of formulations of a water-free, zeolite-based paste. When applied topically it

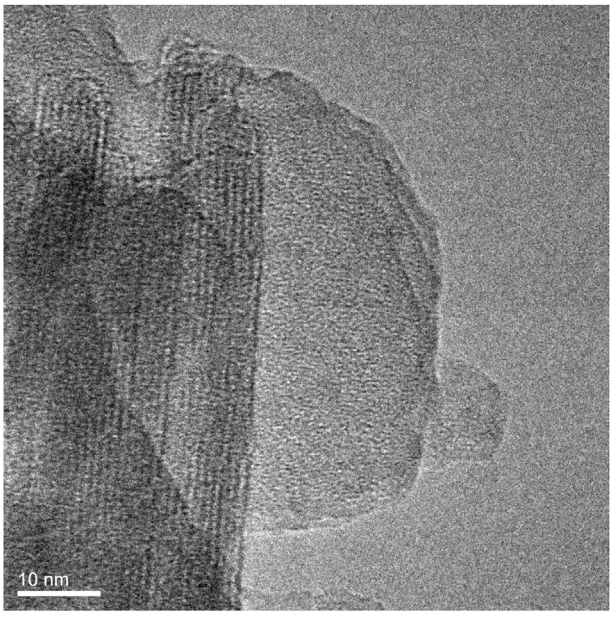

Fig. 3. HRTEM of zeolite from San Andrés, Cuba.

Table 2
Chemical composition of zeolite from San Andrés, Cuba, as determined by XRF (this study) and ICP-OES [10].

Component	XRF	ICP-OES
	wt (%)	
SiO_2	65.3	66.0
TiO_2	0.2	0.3
Al_2O_3	11.2	10.0
Fe_2O_3	1.6	1.8
MgO	1.1	1.0
MnO	…[a]	0.026
CaO	2.6	3.2
Na_2O	1.5	2.5
K_2O	1.6	1.6
SO_3	<0.01	0.075
Cl	<0.002	…
F	<0.05	…
LOI	14.7	12.8
Sum	99.8	99.4
	ppm	
As	<3	<5
Ba	736	800
Bi	5	…
Cd	…	<0.4
Ce	<52	…
Co	<6	…
Cr	<11	<5
Cs	<67	…
Cu	47	9.6
Ga	10	…
Hf	<15	…
Hg	…	<0.05
La	<40	…
Mo	<6	…
Nb	<5	…
Nd	<35	…
Ni	6	<5
Pb	<6	<5
Rb	17	…
Sb	<88	…
Sc	<24	…
Sm	<38	…
Sn	<35	…
Sr	446	…
Ta	<10	…
Th	<6	…
U	<7	…
Zn	…	45

[a] (…) = data not available.

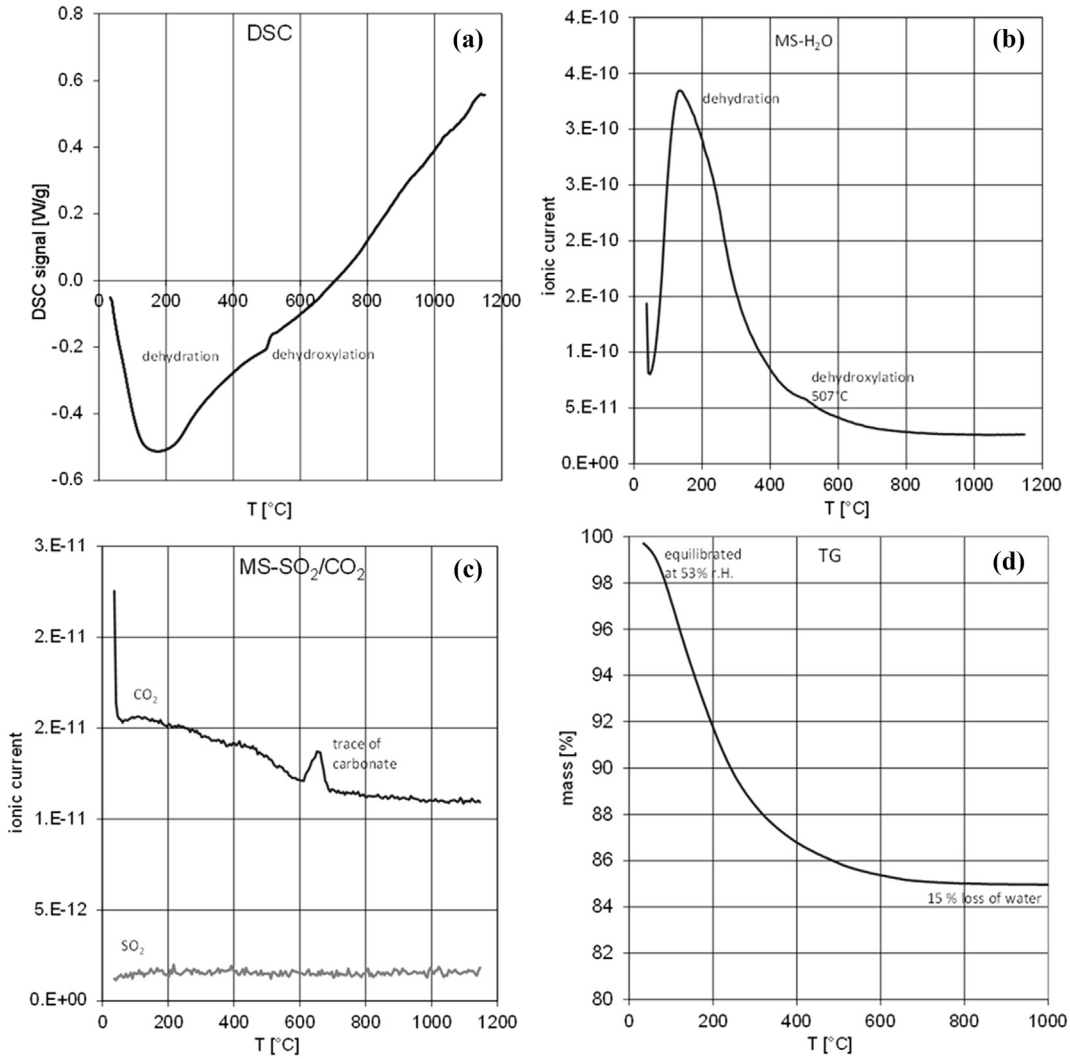

Fig. 4. STA investigation of zeolite from San Andrés, Cuba (a) DSC, b) MS-H_2O, c) MS-SO_2/MS-CO_2, d) TG.

supported healing processes and was attributed *albeit* partially to the inhibition of microbial growth beneath zeolite layers [36].

3.4. Edema and myeloperoxidase content inhibition

Inflammation provoked by TPA resulted in a remarkable edema formation. The application of indomethacin inhibited inflammation almost near completion. Based on MPO activity, the migration of neutrophils remained unaltered (Table 3). These findings were consistent with previous work [16,17,22]. In contrast, early exposure to zeolite caused EI *ca.* 20%. However, EI values increased after 24 h reaching 50%. Thus, zeolite accelerated significantly the normalization of inflamed tissue. These findings coincided with reports for clays and clay minerals [16–22], whereby the anti-inflammatory activity was noted to be surface-mediated.

Trends in EI and MPO content inhibition (CI) appeared not to relate (Table 3). Shortly after exposure, the MPO level increased slightly in relation to the basal value. However, the flux of neutrophils after a prolonged exposure, 24 h, surpassed even the basal values of TPA inflamed tissue. These results were consistent with the idea that zeolite promoted natural tissue repair mechanisms without interfering on neutrophil-based defence processes.

A related report showed that the zeolite sample studied herein adsorbed histamine in as much as 16.0 mg per g [10]. Proposedly, surface charge located at external surface sites (i.e., non-channelled sites) and/or half-cage sites in clinoptilolite or mordenite were accessible to histamine. On the other hand, smectites adsorb amine compounds effectively due to the formation of H-bonding or charge-transfer between amine moieties and siloxane surfaces [37–39]. Pertinent herein is the evidence of TPA and MPO models showing that bentonites (composed primarily by smectites) acted as early anti-inflammatory [20]. Taken together, these studies will help to better understand the effectiveness of applications such as smectite-based treatment of patients with irritable bowel syndrome [40], among others, and therein the need to further scrutinize the role of interactions at the vicinity of siloxane surfaces on the healing properties of clays and clay minerals [18–22,28,41].

The cellular behaviour at the vicinity of mineral surfaces regulating function, growth and survival is surface limited. Primary screening experiments of cell lines [6 cell lines including U251 (central nervous system)] showed that the presence of expandable or non-expandable phyllosilicates inhibited cellular proliferation, consistent with non-specific mechanism(s), whereby structural features common to either group (e.g., siloxane basal planes) may serve as binding site for biomolecules active in the proliferation of

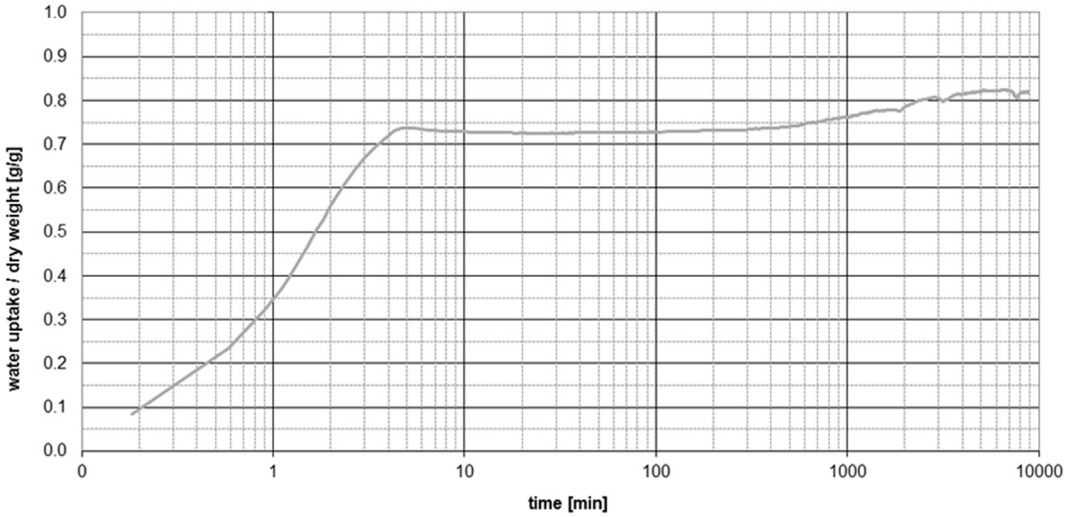

Fig. 5. Water uptake by zeolite from San Andrés, Cuba.

Table 3
Time-dependent edema formation (TPA model) and neutrophil migration (MPO model) under the influence of zeolite. At each ear 1 mg zeolite of grain size ≤50 μm was applied. Experiments were conducted by heptaplicates and reported as average value with standard error including statistical significance at $p \leq 0.01$ (*).

	TPA model			
	$t = 4$ h		$t = 24$ h	
	Edema (mg)	Inhibition (%)	Edema (mg)	Inhibition (%)
Control (no treatment)	0		0	
TPA treatment	16.1 ± 0.7	–	15.7 ± 1.9	
Indomethacin	2.9 ± 0.7*	80.2 ± 5.0*		
Zeolite	12.3 ± 1.0	22.2 ± 6	5.6 ± 2.4*	57.2 ± 18*
	MPO model			
	$t = 4$ h		$t = 24$ h	
	OD_{450nm} biopsy^{-1}	Inhibition (%)	OD_{450nm} biopsy^{-1}	Inhibition (%)
Control (no treatment)	0.034 ± 0.008		0.019 ± 0.008	
Indomethacin	0.02 ± 0.006*	92.5 ± 3.0*		
TPA treatment	0.193 ± 0.017		0.368 ± 0.052	
Zeolite	0.055 ± 0.011*	71.4 ± 6.0*	0.391 ± 0.052	−6.2 ± 14.2

gliomas (e.g., epidermal growth factor receptor), causing the disruption of the cell growth cycle [41]. Likewise, results reported herein for the anti-inflammatory activity by zeolite, primarily as clinoptilolite, $[(Na,K)_{6-2x}Ca_x]$ $(Al_6Si_{30}O_{72})\cdot 24H_2O$, were explained due to the binding of biogenic substances responsible of inflammation (e.g., cytokines, histamine) to structural siloxane domains, by means of multiple π-charge-transfer and/or hydrogen bonding.

4. Conclusions

As determined by a murine inflammation model, using the TPA and MPO methods, zeolite (65% clinoptilolite, 30% mordenite, and 5% smectite) showed antiphlogistic properties. The anti-inflammatory activity was attributed in part to the adsorption of histamine on zeolite. Besides, we do not discard the notion that siloxane surfaces of smectites served also as effective adsorption sites for amine compounds, such as histamine, thereby contributing to abate inflammation.

The inhibition of TPA-inflammatory response by the zeolite sample did not alter the migration of neutrophils, which, after the skin, constitute the primary protection of organisms against pathogens. On the other hand, the formation of edema was reduced by 50% just after 24 h of exposure time while the neutrophil defence mechanisms remained at the level of inflamed tissue. The outcome of this work showed *in-vivo* antiphlogistic properties of zeolite as determined by a murine inflammation model and contributed to a better understanding of oral application in inflammatory bowel diseases [42] and in the topical treatment of inflamed skin with zeolite paste [36].

Acknowledgments

The authors thank Jaime Ortega Lechuga (UAM-Cuajimalpa), Claudia Rivera Cerecedo and Héctor Malagón Rivero (Bioterio, Instituto de Fisiología Celular, UNAM), and Natascha Schleuning (Bundesanstalt für Geowissenschaften und Rohstoffe, BGR) for the assistance; and the Universidad Autónoma Metropolitana for the support (Grant No. UAM-C 33678).

Appendix A. Supplementary data

Supplementary data related to this article can be found at http://dx.doi.org/10.1016/j.micromeso.2016.03.043.

References

[1] T. Andronikashvili, K. Pagava, T. Kurashvili, L. Eprikashvili, Bull. Georgian Natl. Acad. Sci. 3 (2009) 158–167.
[2] M.I. Carretero, C.S.F. Gomes, F. Tateo, in: Clays, Drugs, and Human Health, Developments in Clay Science, vol. 5(5), 2003, pp. 711–764.
[3] G. Cerri, M. Farina, A. Brundu, A. Aleksandra Daković, P. Giunchedi, E. Gavini, G. Rassu, Micropor. Mesopor. Mater 223 (2016) 58–67.
[4] A. Rivera, T. Farías, A.R. Ruiz-Salvador, L.C. de Ménorval, L.C. Micropor, Mesopor. Mater 61 (2003) 249–259.
[5] K. Pavelic, M. Hadzija, in: S.M. Auerbach, K.A. Carrado, P.K. Dutta (Eds.), Handbook of Zeolite Science and Technology, Dekker, New York, 2003, pp. 1143–1174.
[6] C. Colella, Clay Min. 46 (2011) 295–309.
[7] K. Koyama, Y. Takeúchi, Z. Krist. 145 (1977) 216–239.
[8] D.W. Ming, J. Dixon, Clays Clay Min. 35 (1987) 463–468.
[9] H.H. Andersen, J. Elberling, L. Arendt-Nielsen, Acta Derm. Venereol. 95 (2015) 771–777.
[10] T. Selvam, W. Schwieger, W. Dathe, Clay Min. 49 (2014) 501–512.
[11] T.S. Rao, J.L. Currie, A.F. Shaffer, P.C. Isakson, Inflammation 17 (1993) 723–741.
[12] X. Wu, M. Song, K. Rakariyatham, J. Zheng, M. Wang, F. Xu, Z. Gao, H. Xiao, J. Agric. Food Chem. 63 (2015) 10921–10927.
[13] B. Veerapandian, Biophys. J. 62 (1992) 112–115.
[14] W. Somers, M. Stahl, J.S. Seehra, EMBO J. 16 (1997) 989–997.
[15] S.-H. Zhu, L.-J. Zhou, H. Jiang, R.-J. Chen, C. Lin, S. Feng, J. Jin, J.-H. Chen, J.-Y. Wu, J. Zhejiang Univ. Sci. B 15 (2014) 735–742.
[16] H. Cornejo-Garrido, A. Nieto-Camacho, V. Gómez-Vidales, M.T. Ramírez-Apan, P. del Angel-Vicente, J.A. Montoya-de la Fuente, M. Domínguez-López, D. Kibanova, J. Cervini-Silva, Appl. Clay Sci. 57 (2012) 10–16.
[17] J. Cervini-Silva, A. Nieto-Camacho, E. Palacios, A. Montoya, V. Gómez-Vidales, M.T. Ramírez-Apán, Coll. Surf. B 111 (2013) 651–655.
[18] J. Cervini-Silva, A. Nieto-Camacho, M.T. Ramírez-Apan, V. Gómez-Vidales, E. Palacios, A. Montoya, E. Ronquillo de Jesus, Coll. Surf. B 123 (2015a) 1–6.
[19] J. Cervini-Silva, A. Nieto-Camacho, V. Gómez-Vidales, S. Kaufhold, B.K.G. Theng, Appl. Clay Sci. 105–106 (2015b) 48–51.
[20] J. Cervini-Silva, A. Nieto-Camacho, S. Kaufhold, K. Ufer, E. Ronquillo de Jesús, Appl. Clay Sci. 118 (2015c) 56–60.
[21] J. Cervini-Silva, A. Nieto-Camacho, M.T. Ramírez-Apan, in: P. Pasbakhsh, J. Churchman (Eds.), Research Progress in Natural Mineral Nanotubes, Apple Press, New York, 2015d. Ch. 24.
[22] J. Cervini-Silva, A. Nieto-Camacho, E. Palacios, P. del Angel, M. Pentrak, L. Pentrakova, S. Kaufhold, K. Ufer, M.T. Ramírez-Apán, V. Gómez-Vidales, D. Rodríguez Montaño, A. Montoya, J.W. Stucki, B.K.G. Theng, Appl. Clay Sci. 120 (2016a) 101–110.
[23] J. Centner, Atlas of Immuno-allergology, third ed., Hogrefe & Huber Publishers, Göttingen, 1995.
[24] S.J. Klebanoff, Proc. Assoc. Am. Phys. 111 (1999) 383–389.
[25] L.M. De Young, J.B. Kheifets, S.J. Ballaron, J.M. Young, Agents Actions 26 (1989) 335–341.
[26] L.B. Williams, S. Hillier, Elements 10 (2014) 207–211.
[27] K.D. Morrison, R. Misra, L.B. Williams, Sci. Rep. 6 (2016) 19043, http://dx.doi.org/10.1038/srep19043.
[28] E. Juárez, E. Ronquillo de Jesús, A. Nieto-Camacho, S. Kaufhold, E. García-Romero, M. Suarez, J. Cervini-Silva, Appl. Clay Sci. (2016), http://dx.doi.org/10.1016/j.clay.2016.01.034). PII: S0169–1317(16)30035-7.
[29] L.P. Meier, G. Kahr, Clays Clay Min. 47 (1999) 386–388.
[30] S. Kaufhold, R. Dohrmann, Clays Clay Min. 56 (2008) 686–692.
[31] S. Kaufhold, R. Dohrmann, M. Klinkenberg, Clays Clay Min. 58 (2010) 37–43.
[32] M. Merlos, L.A. Gomez, M. Giral, M.L. Vericat, J. Garcia-Rafarell, J. Forn, Br. J. Pharmacol. 104 (1991) 990.
[33] E.E. Bradley, P. Greenspan, J.L. Hargrove, L. Wicker, D.K. Hartle, J. Inflamm. 5 (2008) 149–160.
[34] G.E. Christidis, D.D. Eberl, Clays Clay Min. 51 (2003) 644–655.
[35] D. Vasilev, B. Aleksic, A. Tarbuk, M. Dimitrijevic, N. Karabasil, N. Cobanovic, N. Vasiljevic, Proc. Food Sci. 5 (2015) 300–303.
[36] W. Dathe, OM Ernährung 153 (2015) F3–F7.
[37] G.J. Churchman, B.K.G. Theng, Clay Min. 19 (1984) 161–175.
[38] S.A. Boyd, J.F. Lee, M.M. Mortland, Nature 333 (1988) 345–347.
[39] J.F. Lee, J.R. Crum, S.A. Boyd, Environ. Sci. Technol. 23 (1989) 1365–1372.
[40] F.-Y. Chang, C.-L. Lu, C.-Y. Chen, J.-C. Luo, J. Gastroenterol. Hepatol. 22 (2007) 2266–2272.
[41] J. Cervini-Silva, M.T. Ramírez-Apan, S. Kaufhold, K. Ufer, E. Palacios, A. Montoya, Chemosphere 149 (2016b) 57–61.
[42] G. Glock, EP 2 870 967 A1 (2010) 1-8.